

Journal of Astronomical Telescopes, Instruments, and Systems

AstronomicalTelescopes.SPIEDigitalLibrary.org

Dynamic stabilization of thin aperture light collector space telescope using active rods

Mohit Verma
Adrien Pece
Sylvain Hellegouarch
Jennifer Watchi
Gilles Durand
Simon Chesné
Christophe Collette

SPIE.

Mohit Verma, Adrien Pece, Sylvain Hellegouarch, Jennifer Watchi, Gilles Durand, Simon Chesné, Christophe Collette, "Dynamic stabilization of thin aperture light collector space telescope using active rods," *J. Astron. Telesc. Instrum. Syst.* **6**(1), 014002 (2020), doi: 10.1117/1.JATIS.6.1.014002

Dynamic stabilization of thin aperture light collector space telescope using active rods

Mohit Verma,^{a,b,*} Adrien Pece,^a Sylvain Hellegouarch,^a Jennifer Watchi,^a
Gilles Durand,^c Simon Chesné,^d and Christophe Collette^{a,e}

^aUniversité Libre de Bruxelles, Precision Mechatronics Laboratory, BEAMS Department,
Brussels, Belgium

^bCSIR Structural Engineering Research Centre, CSIR Campus, Chennai, India

^cCEA Saclay, Gif sur Yvette cedex, France

^dUniversité de Lyon, CNRS INSA-Lyon, Villeurbanne, France

^eUniversity of Liège, Department of Aerospace and Mechanical Engineering, Liège, Belgium

Abstract. Thin aperture light collector (TALC) is the next generation of telescopes for space exploration. TALC consists of deployable annular segmented mirrors supported on a central mast with the help of cables. The dynamic stability of the telescope is of immense importance in order to make sure that the telescope is pointing in the right direction during the observation period. We present a control strategy for the dynamic stabilization of the segmented TALC structure using active rods. The active rods consist of collocated pairs of piezoelectric stack actuators and sensors. Decentralized integral force feedback is proposed to enhance the dynamic stability of the TALC. The effectiveness of the strategy is demonstrated on a 1/10th scaled mock-up model of the TALC. For numerical investigation, finite element analysis of the TALC is carried out and a reduced order model is extracted using the Craig–Bampton method. This reduced order model is then used for the design and numerical validation of the controller. Experiments are conducted on the mock-up model of the TALC to evaluate the performance of the proposed strategy. It is found that the proposed strategy is quite effective for dynamic stabilization of TALC. It is found to reduce both steady state and transient responses of the TALC. © 2020 Society of Photo-Optical Instrumentation Engineers (SPIE) [DOI: [10.1117/1.JATIS.6.1.014002](https://doi.org/10.1117/1.JATIS.6.1.014002)]

Keywords: deployable telescope; active control; piezoelectric; integral force feedback; vibration.

Paper 19113 received Oct. 19, 2019; accepted for publication Jan. 21, 2020; published online Feb. 11, 2020.

1 Introduction

In order to continue the exploration of the universe using the far infrared spectrum, larger space telescopes are required. The lesson learned from the James Webb Space Telescope (JWST)¹ are that this exploration will remain affordable only if a disruptive technology emerges, allowing to combine a very large aspect ratio from folded to deployed configuration, and a reliable deployment concept. Toward this purpose, the thin aperture light collector (TALC) project is currently under study by a European consortium.^{2–4} The general structure of the TALC is one of a bicycle wheel. The diameter of the annular mirror of the TALC is 20 m after deployment. The annular mirror is divided into different segments. The topology of the TALC (based on stacking) allows its storage in the fairing of Ariane 6. A pantograph scissor mechanism is used for deployment of the segmented mirror from a stack to form a parabolic ring. The mechanism maintains high stiffness in the TALC during the deployment process. The mirror segments are connected to the central mast of the telescope with the help of cables, similar to the spokes in a bicycle. The final shape of the mirror relies on active controls at various scales in dimension. At a scale below the size of the segment, the shape of an individual segment is adjusted using piezoelectric unimorph control of tens to thousands of pixels.⁵ At mid-scale, actuators placed at the hinges

*Address all correspondence to Mohit Verma, E-mail: mohitverma@serc.res.in

of the segments allow the adjustment of the front wave difference from one segment to another. At large scale, the cable spokes are trimmed in length for both static and dynamic control of the wave front. The actuators used to trim the M1 mirror are comprised of both memory shape piezoelectric actuators and real-time controlled piezoelectric actuators. These piezoelectric actuators can be used from room temperature down to 25 K.

The advancement in space technology demands large aperture telescopes with high resolution. The pointing stability of Hubble Space Telescope is 0.007 arcsec⁶ while that of JWST is 0.004 arcsec.⁷ The pointing stability of a telescope is largely affected by the microvibrations caused due to the on-board equipment.^{8–10} Passive vibration isolation is often used because of the issues such as reliability and low maintenance cost.^{11–14} Owing to the large aperture, space limitations in the launch vehicle, and deployment mechanism, the TALC is bound to be more flexible than the previous telescopes. TALC comprises long cables in the vacuum and long masts that are not easily passively damped in the vacuum. For this reason, an active damping system that can be tuned to the specific optical requirements is deemed more suitable. Many researchers have used active control strategies to improve the precision accuracy of the telescope.^{15–18}

In this paper, we present a strategy for the active damping of the TALC using active rods consisting of piezoelectric stacks. The control strategy is verified both numerically and experimentally. A finite element (FE) model of the TALC is developed with commercial software. The FE model is validated by comparing the results of the modal analysis obtained numerically with the experiments. After validation, a reduced order model is extracted from the FE model using the Craig–Bampton method. Decentralized integral force feedback is used to damp the response of the TALC. The effectiveness of the control strategy is demonstrated on the reduced order model. This strategy is then experimentally verified in the laboratory. A mock-up model of the TALC, scaled to 1/10th of its original size, is fabricated. The performance of the proposed stabilization strategy is evaluated for both steady state and transient responses of the TALC. The organization of the paper is as follows. The concept of TALC is described in Sec. 2. The details of the mock-up model constructed for the laboratory demonstration are presented in Sec. 3. The procedure of the FE modeling and analysis is presented in Sec. 4. The strategy for active control is outlined in Sec. 5. The experiments carried out for the laboratory demonstration of the control strategy are presented in Sec. 6, followed by concluding remarks in Sec. 7.

2 TALC Concept

The different stages in the deployment of the TALC are shown in Fig. 1. In the figure, for the sake of demonstrating the deployment mechanism, the annular mirror is shown to be supported

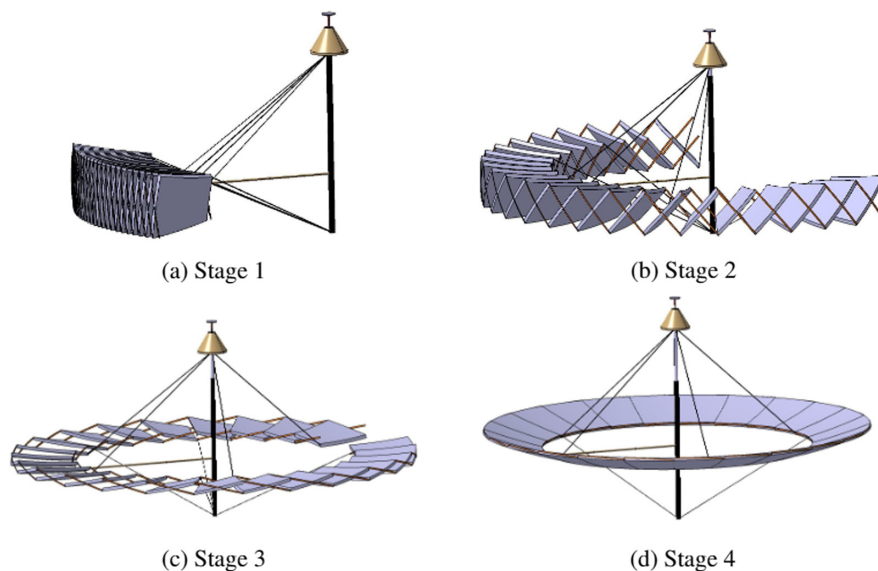


Fig. 1 Different stages in the deployment of TALC.

by only eight cables. However, the actual TALC will have more cables to support the annular mirror assembly. The main topological features of the TALC are:

- TALC is based on an innovative concept of deployable mirror topology based on stacking, unlike folding, which is conventionally used. The reason for choosing such a topology is that it allows maximizing the ratio of the deployed surface to the storage volume.
- The primary annular mirror in the TALC is segmented. The segments of the mirror are made up of electro-deposited nickel, carbon composite, and honeycomb stacks. The segments are identical and hence can be produced economically.
- The segmented mirror parts are held in place using a tensegrity structure similar to that of a Ferris wheel. The spokes of the tensegrity structure consist of cables that are wound on a winch. These spokes are then connected to the central mast, which forms the telescope axis.
- A pantograph scissor system is used for the linking of the segmented mirrors. The system ensures high stiffness during the deployment of the stacked segmented mirrors to form a primary annular mirror.
- The shape of the mirror is controlled using active optics with in-plane forces. This avoids the need for a rigid structure as required in shape control using normal forces.

The measurement accuracy of the telescope is directly related to the manufacturing precision and its dynamic stability. Usually, for infrared observation, the shape variation (due to the manufacturing process) has to be lower than $3 \mu\text{m}$. These requirements can be reached using various control devices. The final TALC telescope will present three main active control systems. In the first system, active cables¹⁹ are used to damp the vibrations of the telescope. Previous study has shown the efficiency of the system using only eight active cables in addition to passive cables.²⁰ It was found that the amplitude of the disturbances was reduced by a factor of 3. The second active control system consists of piezoelectric patches distributed inside the mirrors. These patches are then actuated to correct the shape of the mirrors. This will mainly be used to correct manufacturing defects and/or thermal effects on the shape of the mirrors.²¹ The present study focuses on the third type of active control system, which also aims at damping the vibration response of the TALC. The system consists of the active rods linking the segmented mirrors on the external ring (see Figs. 2 and 5). The rods (allowing for adjustment of the length) are in series with the transducer device (shown in Fig. 4).

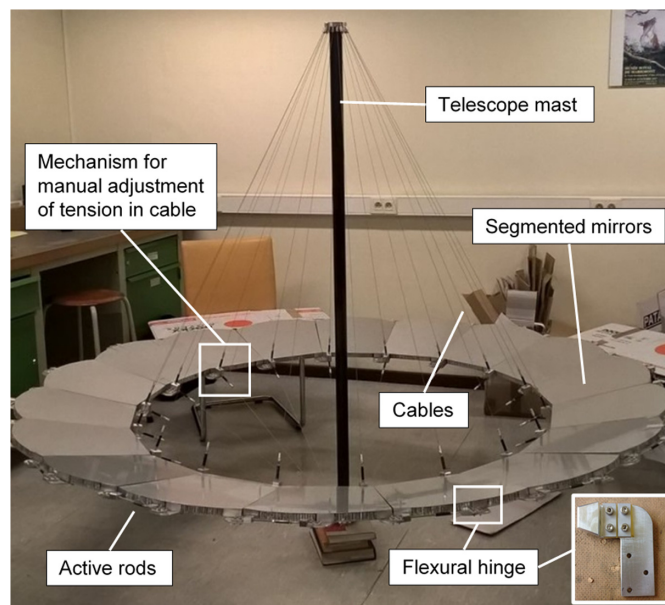


Fig. 2 One-tenth scaled mechanical mock-up model of the TALC.

3 Mock-Up Model of TALC

The TALC is a complex structure to study in the laboratory, mainly due to its size and the Earth's gravity. Indeed, the TALC is designed to work in a zero-gravity environment. In such conditions, mechanical design constraints are drastically different from the usual ones, especially regarding the size of the structure. In order to carry out the experiments in the laboratory, a 1/10th scaled mock-up model of the TALC (in the deployed state) is fabricated (Figs. 2 and 5). The mock-up model is made of aluminum. Carbon fiber-reinforced plastic (CFRP) is used for the mast of the telescope. Each of the segmented annular mirrors is fabricated as a honeycomb sandwich structure. The assembly of the TALC is carried out using the following steps:

- (i) The brass flexural hinges are attached to each of the segmented mirrors.
- (ii) The segmented mirrors are then attached to each other using the brass fixtures to form a circular assembly.
- (iii) The mast of the telescope is placed in the center and the segmented mirrors are attached to it with the help of cables.
- (iv) The model is first mounted without actuators. The adjacent segmented mirrors are attached with rigid threaded rods.
- (v) Some of the threaded rods are then replaced by active rods (piezoelectric stack actuators and sensors).

In order to have a good representation of the dynamics of the full-scale structure, it is important to ensure that the structure is balanced. The structure of the TALC is balanced by adjusting the tensions of the cables connecting the segmented mirrors with the mast of the telescope. Since the TALC is axisymmetric, the lengths of the top cables are the same. The mass is also equally distributed. The structure is said to be balanced when all the top cables have equal tension. This also implies that the tension values in all the bottom cables are also equal. The tension in a cable is indirectly calculated from its first harmonic frequency. The first harmonic frequency of the cable in tension can be written as

$$f = \frac{1}{2\pi} \sqrt{\frac{T}{\mu}}, \quad (1)$$

where f is the frequency of the first harmonic in Hz, T is the tension in the cable, and μ is the mass per unit length of the cable. The tension in each of the cables is adjusted until their first harmonic reaches the desired value (which is obtained using the tension in the cable obtained analytically and is described in the next section). In this way, it is ensured that the mock-up model of the TALC is perfectly balanced. The test setup used for identifying the harmonics of the cable is shown in Fig. 3. The setup consists of a laser beam and a photodiode. The vibrations of the cable block the laser beam directed on a photodiode. This changes the voltage output of the photodiode. The frequency of the fluctuation in the voltage signal corresponds to the frequency of the harmonics of the cable.

Active rods are installed between the adjacent segmented mirrors. These rods are equipped with piezoelectric stack transducers APA100M from Cedrat Technologies (similar to flexural-mode piezoelectric actuators).²² The stack is further divided into two parts. One stack is used as an actuator while the other is used as a force sensor. Figure 4 shows the transducers used in the active rods.

4 FE Modeling and Analysis of TALC

Figure 5 shows a computer aided design (CAD) view of the 1/10th scaled mock-up model of the TALC, connected to a central mast with 36 cables (18 to each end of the mast). The picture also shows a close-up view of one of the active rods connected to adjacent annular mirror segments. The FE model of the mock-up TALC is developed by importing the CAD models of the various parts created in CATIA. These parts are then assembled to rebuild the model in ABAQUS, which is later used for the analysis. It is important to note that the aim of the FE analysis is not to have

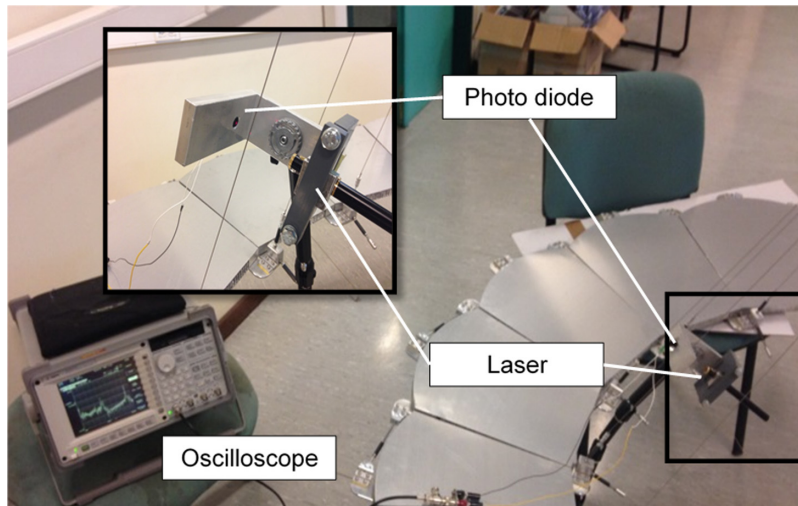


Fig. 3 Test setup used for the adjustment of the tension in the cable. The harmonics of the cable are observed by fluctuations in the voltage across the photodiode.

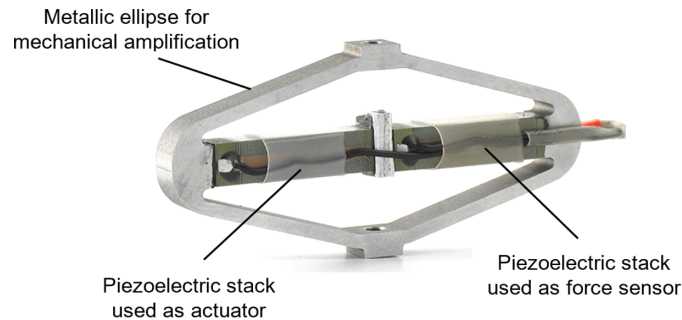


Fig. 4 Transducer used in active rods: one piezoelectric stack is used as an actuator while the other is used as a force sensor.

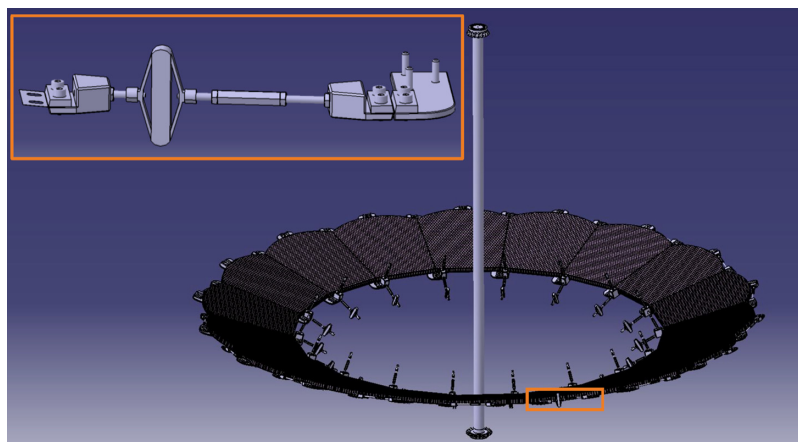


Fig. 5 CAD model of the 1/10th scaled mock-up TALC. The model includes a representation of the mirror segments, cables, and connections. A close-up view of the active rod is shown on the top left.

an accurate model of the mock-up TALC. The aim is to arrive at an approximate and computationally inexpensive model of the TALC, which can aid in the task of controller design and verification before the actual experiments. In this section, we describe the modeling details and assumptions made for FE analysis.

4.1 Actuators

The geometry of the actuator is extracted from the datasheet. The piezoelectric stacks are represented by a stiffness element inside the ellipse. The stiffness of the piezoelectric stack is obtained from the manufacturer and is also analytically verified based on the geometry and the material properties of titanium lead zirconate. The stiffness of the piezoelectric stacks used in the simulation is 48,000 N/mm.

4.2 Cables

The 36 cables in TALC are modeled using a stiffness element. The stiffness of the cables is determined assuming that the TALC is balanced. The geometry of the TALC from the top and side views is shown in Fig. 6. It is assumed that the TALC is suspended horizontally on two soft springs. The weight of the mirrors (P) is assumed to be uniformly distributed. Based on the figure, the tension in the cable (at node 2) can be written as

$$\begin{aligned} \vec{T}_{21} &= -T_{21} \cos(\alpha) \sin(\beta) \vec{x} + T_{21} \sin(\alpha) \sin(\beta) \vec{y} + T_{21} \cos(\beta) \vec{z} \\ \vec{T}_{22} &= -T_{22} \cos(\alpha) \sin(\theta) \vec{x} + T_{22} \sin(\alpha) \sin(\theta) \vec{y} - T_{22} \cos(\theta) \vec{z}, \end{aligned} \tag{2}$$

where T_{21} and T_{22} represent the tension in the cables above and below the mirror, respectively. For angles α , β , and γ , see Fig. 6. Using the equilibrium of forces in the Y direction

$$T_{21} \sin(\alpha) \sin(\beta) + T_{22} \sin(\alpha) \sin(\theta) = P_2, \tag{3}$$

where P_2 is the component of the weight acting at node 2. The equilibrium along the mast can be written as

$$T_{21} \cos(\beta) = T_{22} \cos(\theta). \tag{4}$$

Solving the above two equations, we get

$$T_{21} = T_{22} \frac{\cos(\theta)}{\cos(\beta)}, \quad T_{22} = \frac{P_2}{\sin(\alpha) [\tan(\beta) \cos(\theta) + \sin(\theta)]}. \tag{5}$$

Using the above equations, the values of T_{21} and T_{22} are found to be 39.3 and 85.5 N, respectively. Since the TALC is assumed to be balanced, the tension in the other cables at the top and bottom of the mirror is equal to those evaluated at node 2.

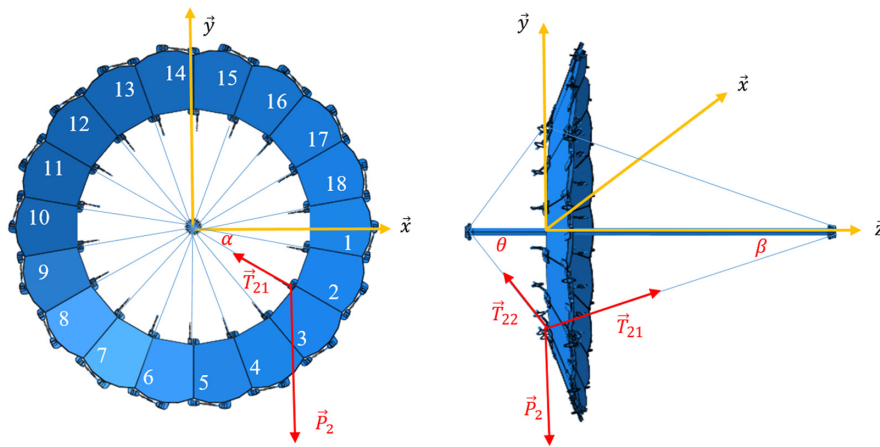


Fig. 6 Force equilibrium in TALC. The tension in the cables of the TALC is calculated by assuming that the mast of the telescope is suspended horizontally and is supported by two soft springs at its end.

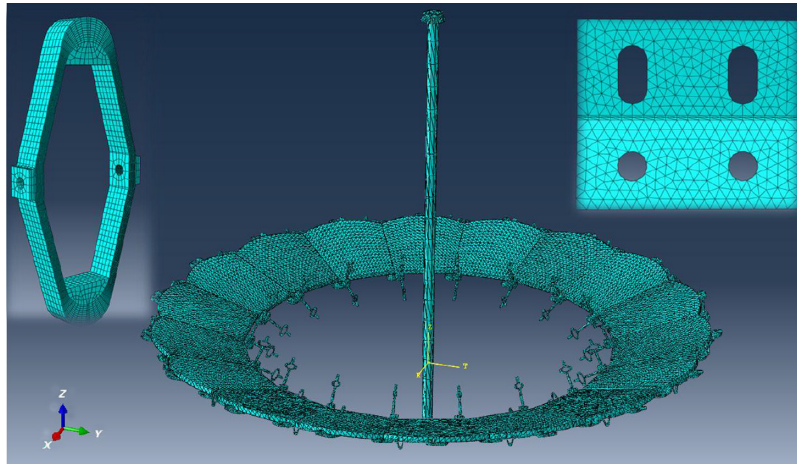


Fig. 7 Meshing used for the FE analysis of the TALC assembly. The top left shows the meshing used for the actuator while the top right shows the meshing used for the flexible hinge.

4.3 Telescope Mast

The mast of the telescope is modeled as a three-dimensional deformable solid. The material properties of high-strength carbon fiber are assigned to the mast. For simplification, the CFRP is idealized to have homogeneous elastic properties in all directions.

4.4 Segmented Mirrors

The mirror of the telescope has a complex geometry. It is made up of a honeycomb sandwich structure, which is not only difficult to model, but is also computationally expensive. Since we are not interested in the flexible modes of the mirror, we model it as a solid panel with the equivalent homogenized material properties. The density of the material is estimated by first calculating the volume from the CAD model and then dividing it by the weight (obtained by weighing in the laboratory).

4.5 Meshing and Boundary Conditions

The different parts of the TALC FE model are meshed either with a hexahedral or tetrahedral mesh. The hexahedral mesh is modeled with C3D8R (available in the ABAQUS element library) which is an eight-node linear brick element with reduced integration and hourglass control. The tetrahedral mesh is modeled using C3D10 (available in the ABAQUS element library), which is a 10-node quadratic tetrahedron element. The model after meshing has about 13 million degrees of freedom. An illustration of the meshed TALC assembly is shown in Fig. 7. In a real space situation, the telescope would be totally free from any external mechanical stress. But in order to eliminate the rigid modes, a fixed boundary condition is applied at the origin of the coordinate axes shown in Fig. 7. All the materials of the TALC are assumed to be perfectly elastic for the sake of simplicity.

4.6 Numerical Modal Analysis

It is important to verify that the mock-up model of the TALC is a good representative of the actual TALC. This is done by carrying out the modal analysis of the mock-up and actual TALC models. The first 20 modes of the models below 100 Hz are extracted. It should be noted that the mock-up model cannot be an exact scaled copy of the actual TALC. Various components, such as transducers, clamping system, central beam, connection devices, etc., cannot be perfectly scaled. A comparison between the full scale and the mock-up structure is shown in Fig. 8. The modal frequencies of the mock-up model are found to increase by a factor between 5 and 10. This is attributed to the fact that the geometrical parameters are scaled by a factor of 10 in the mock-up

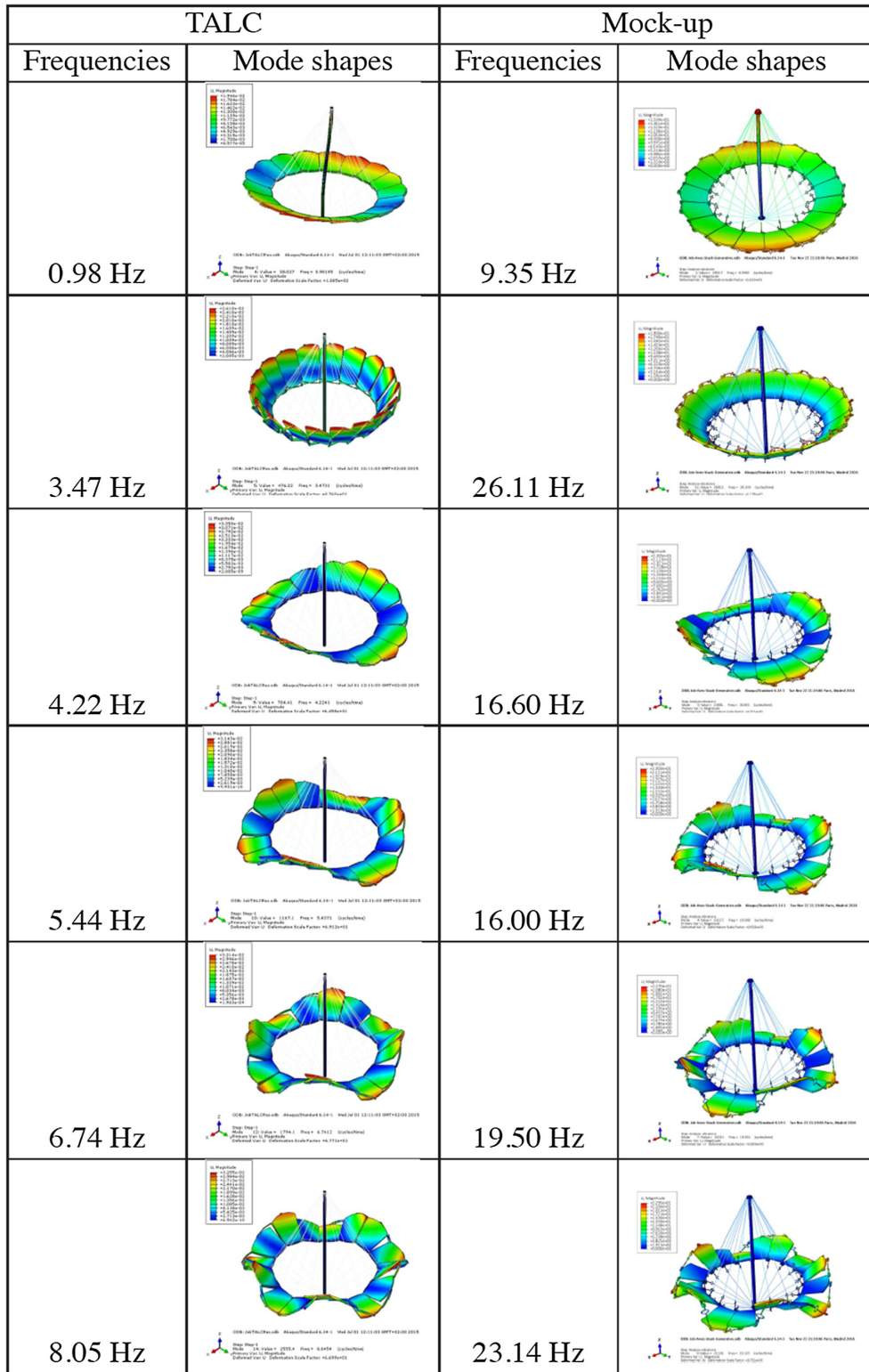


Fig. 8 Comparison of mode shapes and their frequencies for the actual and mock-up TALC.

model, which increases the resonance frequency. More on similarity laws in mechanical systems can be found in Ref. 23. It is worth pointing out that these variations in the modal frequencies will not affect the control authority and efficiency of the proposed stabilization strategy. The important observation is that the shape and the order of modes are matching. Also, the strain distributions in the mode shapes are similar and hence, the control device will demonstrate a

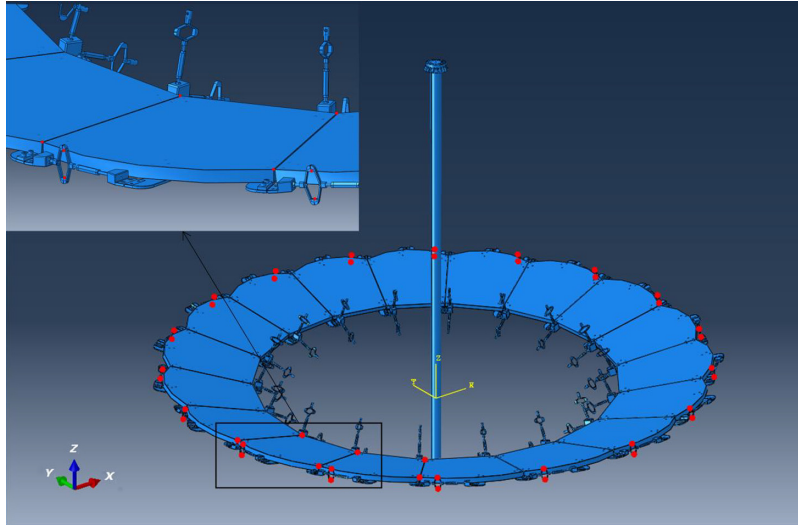


Fig. 9 Nodes retained for model order reduction.

similar performance. Without the loss of generality, it can be assumed that the active control strategy that works for the mock-up model will work for the actual TALC as well.

4.7 Model Order Reduction

The next step is the model order reduction. It is difficult to design a control strategy with a model having around 13 million degrees of freedom. In order to simplify the task of controller design and to reduce the computational cost, model order reduction is carried out using the Craig–Bampton method.²⁴ This method is well known and highly effective for model order reduction. It makes it possible to decompose the overall behavior of a structure, or an assembly of substructures, into the sum of the first vibratory modes of the structure or of each substructure. The model after reduction contains the physical degrees of freedom of interest and is called a superelement. The first step is to select a group of condensation nodes and save them in a set within the ABAQUS model. These nodes are those we wish to observe after reduction (six nodes of observation on the mirrors), and to which we will apply the control forces (one node at each end of the springs in the actuators and 36 nodes in total). The initial force in the piezoelectric stack due to the stiffness will be added to the active control force. The nodes selected for condensation are shown in Fig. 9.

5 Strategy for Active Control

Figure 10 shows the schematics of the resulting transducer system. The model leads to the following equation:

$$F_a + F_s = kdx, \quad (6)$$

where F_a is the force generated by the actuator, F_s is the measured force, k is the mechanical stiffness of the stacks, and dx is the length variation. The control law used is decentralized integral force feedback.²⁵ It offers the advantages of robustness and simplicity. The control law can be written as

$$F_a = -\frac{g}{s}F_s = H_{\text{IFF}}(s)F_s, \quad (7)$$

where s is the Laplace variable and g is the loop gain. It is a single tunable parameter that can be adjusted to optimize the damping. The resulting transfer function of the transducer is

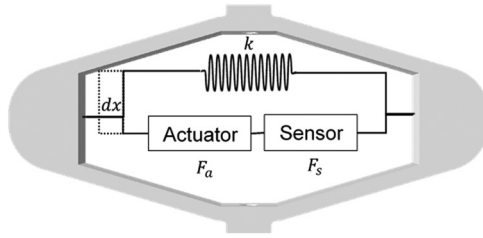


Fig. 10 Schematics of the transducer used in the active rods.

$$H(s) = \frac{F_s}{dx} = \frac{k}{1 + H_{IFF}(s)}. \tag{8}$$

This transfer function will be in feedback with the reduced model of the mock-up TALC used to simulate the structure with an active control device. The gain g is set to 500 and is found to be effective in damping the first few modes of the mock-up TALC. The block diagram of the numerical implementation of the active control strategy is shown in Fig. 11. The reduced order model obtained using the Craig–Bampton method is in a Cartesian frame. The outputs of the model are transformed to the local coordinates of the actuator by multiplying it by the Jacobian matrix (J). The output of the controller is again multiplied with the transpose of the Jacobian (J^T) in order to transform the control force to the Cartesian frame. The responses of the mock-up TALC model with and without control are compared in Fig. 12. This performance is obtained with 18 rods distributed between the mirror segments. It is found that the first two modes that appear around 9.4 and 16 Hz are drastically damped. The results are promising for the future control of the TALC. In the next section, experiments are conducted on the mock-up TALC model in order to verify the effectiveness of this control strategy.

6 Experimental Investigations

The test setup used for the experimental investigations is shown in Fig. 13. The mock-up model of the TALC is kept in an inclined position. The bottom of the telescope mast is kept on the ground while the top of the mast is restrained vertically using two cables. Only six active rods are used between the adjacent segmented annular mirrors. Before the beginning of the experiments, it was made sure the TALC was balanced by manually adjusting the tension in the cables using the procedure described in Sec. 2. The experiments are carried out in three different stages. In the first stage, the mode shapes of the mock-up TALC are evaluated experimentally.

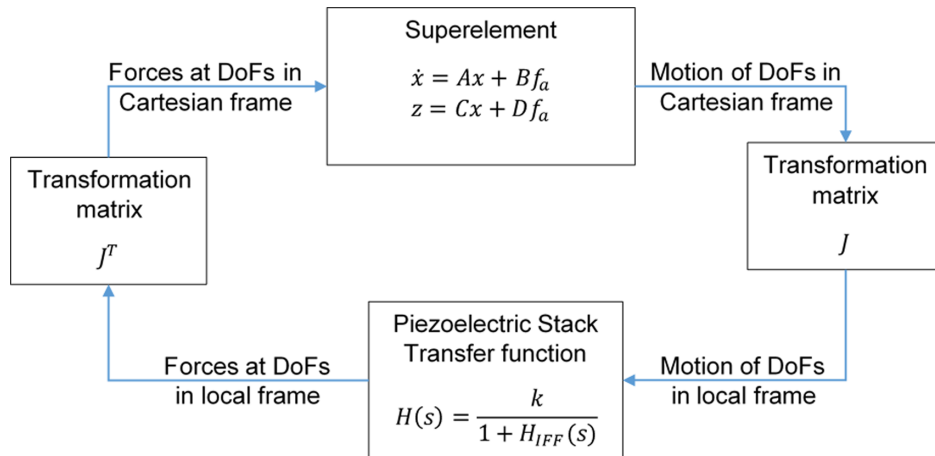


Fig. 11 Block diagram for the numerical implementation of the control strategy proposed for the active stabilization of TALC.

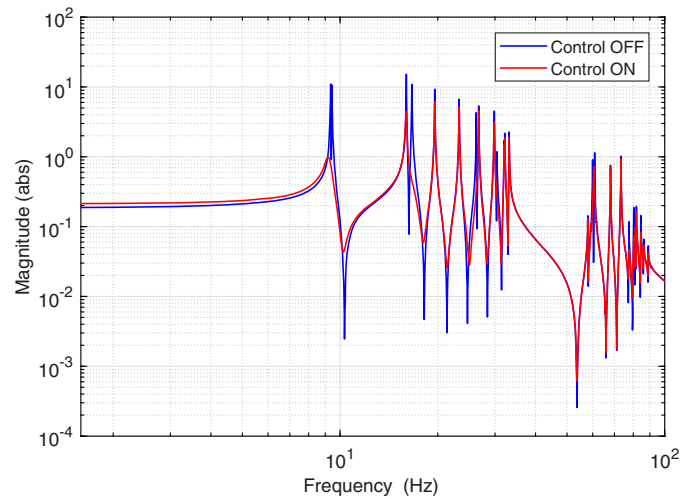


Fig. 12 Compliance of one point (similar to index 5 in Fig. 14) in the direction perpendicular to the mirror plane obtained using a reduced order model with and without active control.

The mode shapes thus obtained are compared with those obtained from the FE model. In the second stage, the experiments are conducted with the controller designed in the previous section. The responses with and without active control are compared to see the effectiveness of the proposed strategy. The third stages of the experiments focus on the transient response of the TALC. The effectiveness of the control strategy in reducing the transient response of the TALC is studied using an impact hammer.

6.1 Experimental Modal Analysis

In order to have good estimation of the mode shapes, it is necessary to excite the structure at all frequencies (more importantly frequencies < 100 Hz). Only one of the active rods was used to excite the entire mock-up TALC model. The motion of the structure is measured using laser scanning interferometer (Polytec OFV 400). The points whose motions are scanned by the interferometer are shown in Fig. 14. Four points are selected on each of the segmented mirrors in order to capture the rigid body motion. To obtain good results, the mirror surface should be

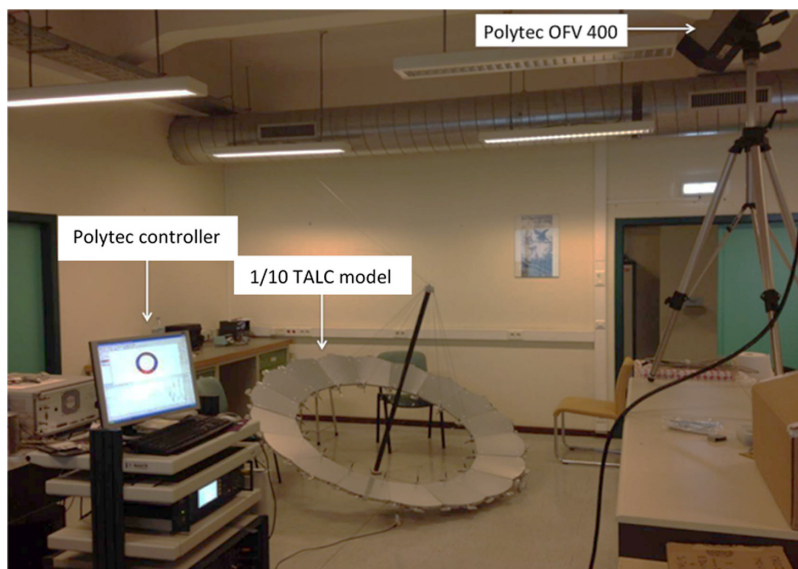


Fig. 13 Picture of the experimental setup and instrumentation used to measure the response of the mock-up TALC.

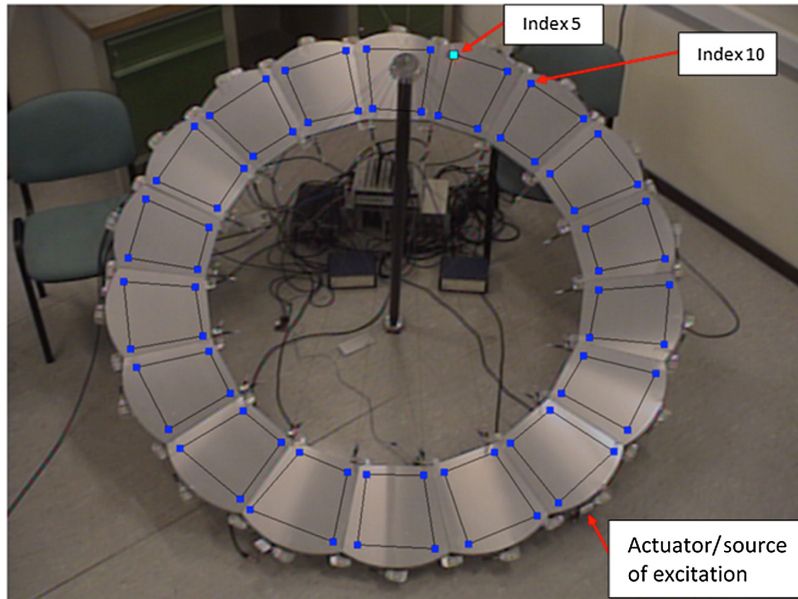


Fig. 14 Network of points scanned by the interferometer (Polytec OFV 400).

perpendicular to the laser scanner. White noise is injected in one of the active rods and the motion of the points on the segmented mirrors is recorded. The comparison of the first eight-mode shapes obtained numerically and experimentally is shown in Fig. 15. The figure shows the modal frequency, measured mode shape (along with its simplified representation), and the corresponding mode obtained from the FE model. It can be seen that modes 1 to 4 and 7 to 8 match well with those obtained from the FE model while modes 5 and 6 do not match well. This may be due to the local variation in the stiffness of the flexural hinges used to connect the adjacent mirror or due to the approximations made in the modeling. These discrepancies in the modal frequencies will not affect the inferences drawn from the experiments conducted on the mock-up TALC.

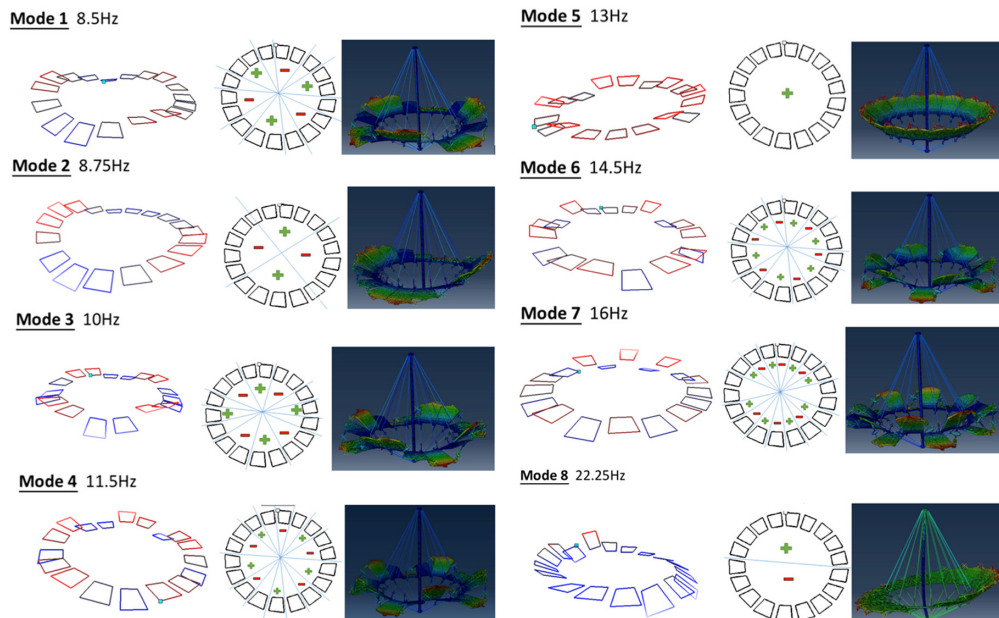


Fig. 15 Comparison of numerical and experimental shapes for eight modes contained in the frequency range of interest, i.e., between 5 and 50 Hz. For each mode, the sketch on the left shows the mode shape measured experimentally, the center shows the simplified version of the experimental mode shape, and the right shows the shape obtained from the FE model.

The modes of the TALC that are targeted to damp using active control are also the modes of the mock-up TALC.

6.2 Active Control

In this stage of the experiments, we use the decentralized integral force feedback to damp the response of the mock-up TALC. The gain value is set the same for all the active rods. The control law is implemented in real-time using dSpace. As a first step, we compare the effect of control on the motion of points 5 and 10 (see Fig. 14). The magnitudes of the vibration signal measured by the scanner at points 5 and 10 are compared in Fig. 16. The frequency resolution of the response was limited by the scanner used for recording the motion. It can be observed that the active control exhibits a similar performance at both points. The aim of this exercise is to demonstrate that the effectiveness of the control strategy can be observed at any point regardless of its location. In the next step, we study the effect of the number of active rods on the vibration control of the mock-up TALC. The experiments are carried out by gradually increasing the number of active rods from one to six. The responses of the TALC model with the different number of active rods are compared in Fig. 17. It can be seen that the damping performance is improved

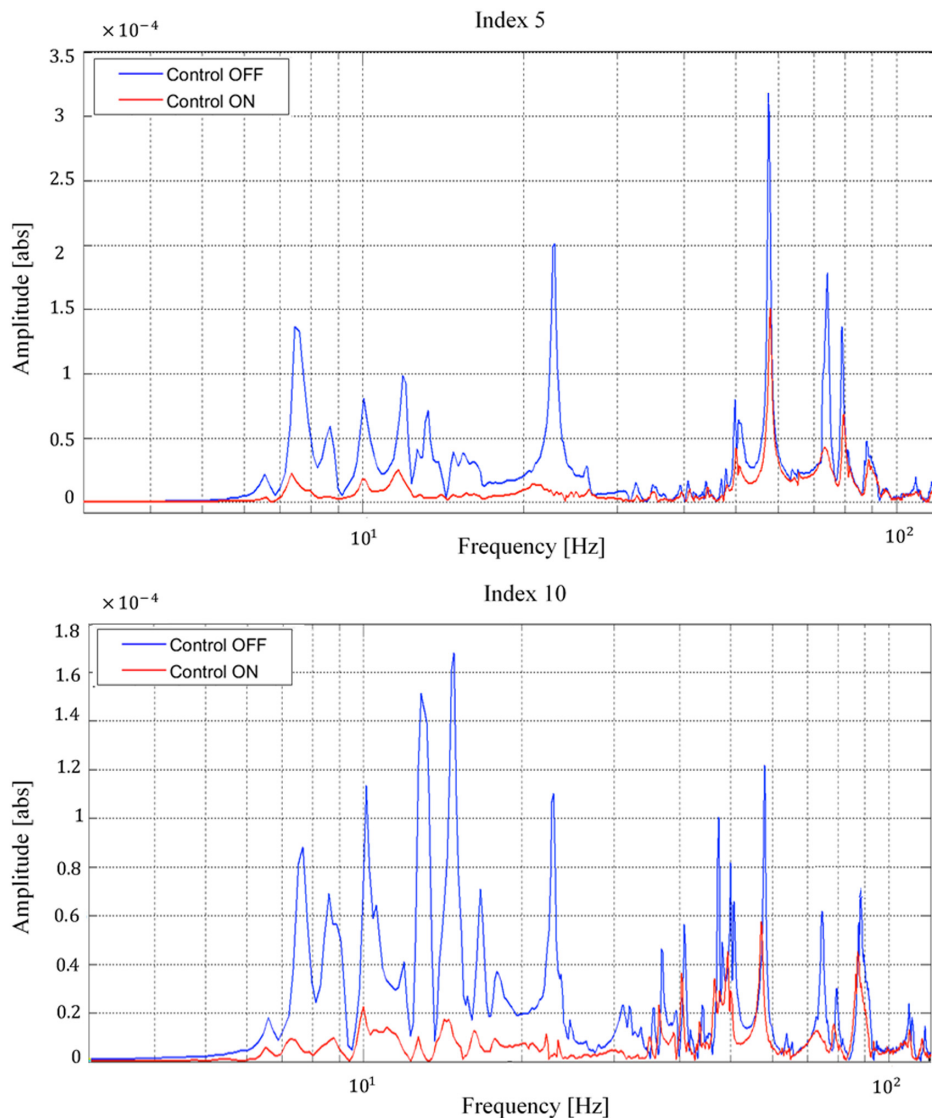


Fig. 16 Frequency response of the vibration measured by the scanner, recorded at points 5 and 10 (see Fig. 14) with and without integral force feedback.

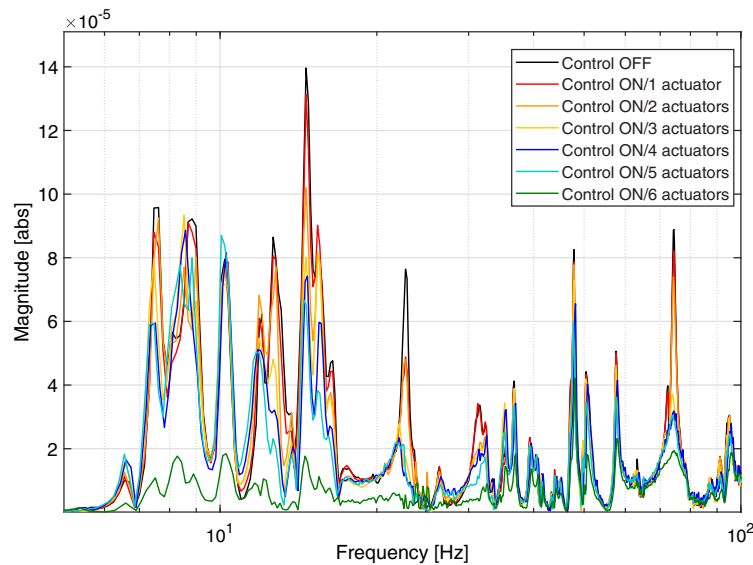


Fig. 17 Effect of the number of active rods on the frequency response of the mirror.

drastically with the increase in the number of active rods. Also, the control strategy is able to damp most of the modes by a factor ranging from 2 to 10. The variation in the root mean square (rms) of the magnitude with the number of active rods is given in Table 1. It is observed that six active rods result in a response reduction by 66%. Based on the desired level of damping, the number of active rods and controller gains can be optimized. Since it is not the main focus of this study, this task is not pursued any further and will be the focus of future studies.

6.3 Impact Hammer

TALC in space might be subject to forces that disturb its steady state or equilibrium. It is important to ensure that the transient response does not cause any damage to the mirrors and the cables of the TALC. In order to study the effect of the active control strategy in reducing the transient response of the TALC, experiments are conducted using an impact hammer. In impact hammer testing, the structure is excited with a hammer instrumented with a force transducer. The transient response of the TALC is recorded using an interferometer. At first, the transient response of the TALC is recorded when the active controls are off. This response is then compared with the transient response recorded when the active controls are turned on. It was ensured that the TALC was excited with the same level of force in the experiments carried out with the impact hammer. The transient responses of the mock-up TALC with and without control are compared

Table 1 Variation of rms of the mock-up TALC response with the number of active rods.

Number of active rods	rms of response	Percentage reduction in response
0	2.71×10^{-6}	—
1	2.57×10^{-6}	5%
2	2.38×10^{-6}	12%
3	2.09×10^{-6}	23%
4	1.94×10^{-6}	28%
5	1.85×10^{-6}	32%
6	9.21×10^{-7}	66%

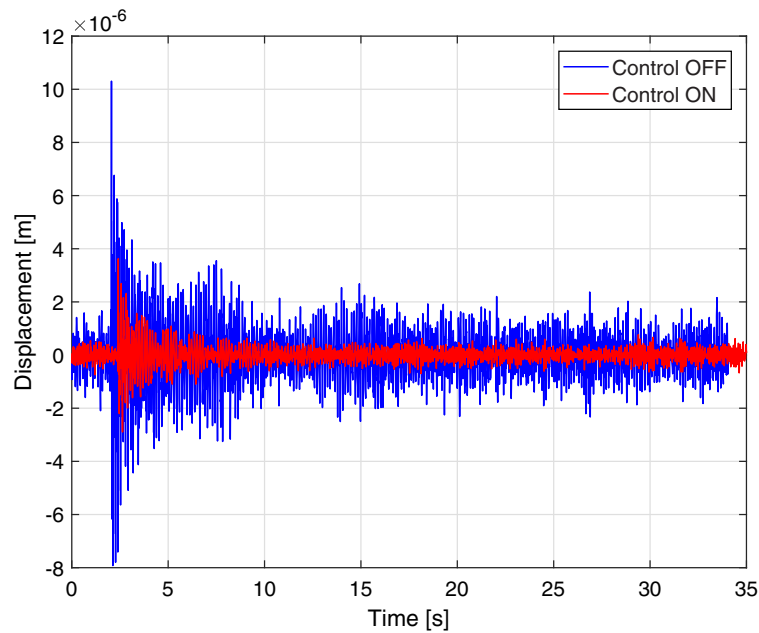


Fig. 18 Hammer impact response when the control is turned OFF (blue curve) and ON (red curve). The transient response is reduced by nearly 70%.

in Fig. 18. It is observed that the proposed strategy is quite effective in reducing the transient response of the TALC. The rms of the response reduced from $3.3295 \cdot 10^{-5}$ m to $1.091210 \cdot 10^{-6}$ m when the active control is switched on. Active rods are able to reduce the transient response by nearly 70%.

7 Concluding Remarks

A strategy for dynamic stabilization of the TALC using active rods has been presented in this paper. The active rods consist of collocated pairs of piezoelectric actuators and sensors. These active rods are inserted between the adjacent pairs of a segmented annular mirror. The mock-up model of TALC, scaled to 1/10th of its original size, was fabricated for the laboratory demonstration of the control strategy. The FE modeling and analysis of the TALC has been carried out with commercial software. The FE model is then verified by comparing the results of the numerical modal analysis with experiments. Decentralized integral force feedback has been proposed to reduce the vibration of the TALC. The control strategy is verified numerically on a reduced order model extracted from the FE model using the Craig–Bampton method. After numerical verification, the experiments are conducted in the laboratory on the mock-up TALC model. The active rods have been found to have significant impact on reducing the response of the TALC. It has been shown that resonance peaks corresponding to deformations of the segmented annular mirror can be damped by up to a factor 10. Such a performance is encouraging for further studies, considering the stringent constraints imposed by the design regarding the number and location of the actuators. Also, the strategy has been found to be quite effective in reducing not only the steady-state, but also the transient response as well.

Acknowledgments

The authors gratefully acknowledge the Brussels Capital Region for funding this research under the program Brains Back to Brussels and also the financial support of the Fonds National de la Recherche Scientifique for funding Christophe Collette. Disclosures: The authors declare no potential conflicts of interest and relevant financial interests with respect to the research, authorship, and/or publication of this article.

References

1. G. S. Wright et al., “The JWST MIRI instrument concept,” *Proc. SPIE* **5487**, 653–663 (2004).
2. M. Sauvage et al., “The science case and data processing strategy for the thinned aperture light collector (TALC): a project for a 20 m far-infrared space telescope,” *Proc. SPIE* **9143**, 91431B (2014).
3. G. Durand et al., “TALC: a new deployable concept for a 20 m far-infrared space telescope,” *Proc. SPIE* **9143**, 91431A (2014).
4. M. Sauvage et al., “A development roadmap for critical technologies needed for TALC: a deployable 20 m annular space telescope,” *Proc. SPIE* **9904**, 99041L (2016).
5. P. Rausch, S. Verpoort, and U. Wittrock, “Unimorph piezoelectric deformable mirrors for space telescopes,” *Proc. SPIE* **9904**, 990468 (2016).
6. J. H. Crocker, “Fixing the Hubble space telescope,” *Proc. SPIE* **1494**, 2–8 (1991).
7. A. J. Bronowicki and J. W. Innis, “A family of full spacecraft-to-payload isolators,” *Technol. Rev. J* **13**, 21–41 (2005).
8. Q. Hu, Y. Jia, and S. Xu, “Adaptive suppression of linear structural vibration using control moment gyroscopes,” *J. Guidance Control Dyn.* **37**(3), 990–996 (2014).
9. Y. Takei et al., “Vibration isolation system for cryocoolers of soft x-ray spectrometer on-board ASTRO-H (Hitomi),” *J. Astron. Telesc. Instrum. Syst.* **4**(1), 1–10 (2018).
10. D. G. MacMartin and H. A. Thompson, “Vibration budget for observatory equipment,” *J. Astron. Telesc. Instrum. Syst.* **1**(3), 034005 (2015).
11. D. Kamesh, R. Pandiyan, and A. Ghosal, “Passive vibration isolation of reaction wheel disturbances using a low frequency flexible space platform,” *J. Sound Vib.* **331**(6), 1310–1330 (2012).
12. L. P. Davis et al., *Hubble Space Telescope Reaction Wheel Assembly Vibration Isolation System*, vol. **9**, NASA Marshall Space Flight Center, Huntsville, Alabama (1986).
13. A. J. Bronowicki, “Vibration isolator for large space telescopes,” *J. Spacecr. Rockets* **43**(1), 45–53 (2006).
14. J. Yang et al., “Design of a vibration isolation system for the space telescope,” *J. Guidance Control Dyn.* **38**(12), 2441–2448 (2015).
15. S. N. Sayapin and Y. N. Artemenko, *Intelligence System for Active Vibration Isolation and Pointing of Ultrahigh-Precision Large Space Structures in Real Time*, pp. 103–115, Springer International Publishing, Cham (2016).
16. Y. Zhang and X. Guan, “Active damping control of flexible appendages for spacecraft,” *Aerosp. Sci. Technol.* **75**, 237–244 (2018).
17. H. Shi et al., “An active control strategy to suppress nonlinear vibrations of large space membranes,” *Acta Astronaut.* **155**, 80–89 (2019).
18. R. G. Cobb et al., “Vibration isolation and suppression system for precision payloads in space,” *Smart Mater. Struct.* **8**(6), 798–812 (1999).
19. R. Nan et al., “Adaptive cable-mesh reflector for the FAST,” *Acta Astronomica Sinica* **44**(2), 13–18 (2003).
20. C. Collette et al., “An active control concept for the talc space telescope,” *Mech. Ind.* **18**(5), 510 (2017).
21. N. Devaney et al., “Development of a prototype active optics system for future space telescopes,” *Appl. Opt.* **57**(22), E101–E106 (2018).
22. H. Wang, “Analytical analysis of a beam flexural-mode piezoelectric actuator for deformable mirrors,” *J. Astron. Telesc. Instrum. Syst.* **1**(4), 049001 (2015).
23. C. Collette, “Usure ondulatoire en transport ferroviaire: mécanismes et reduction,” PhD thesis, Université libre de Bruxelles, Brussels, Belgium (2007).
24. M. C. Bampton and R. R. Craig Jr., “Coupling of substructures for dynamic analyses,” *AIAA J.* **6**(7), 1313–1319 (1968).
25. S. Chesné, A. Milhomem, and C. Collette, “Enhanced damping of flexible structures using force feedback,” *J. Guidance Control Dyn.* **39**(7), 1654–1658 (2016).

Mohit Verma received his PhD in structural engineering from AcSIR, India. After that he joined Precision Mechatronics Laboratory at ULB, Belgium as postdoctoral research associate. He has

been working as a scientist at CSIR–Structural Engineering Research Centre since 2011. His area of interest is vibration control of structures.

Jennifer Watchi received her bachelor's degree in engineering physics and her master's degree in engineering physics, specializing in applied physics, from the Université Libre de Bruxelles in 2013 and 2015. Since 2015, she has been a doctoral candidate at the Precision Mechatronics Laboratory.

Simon Chesné received his MSc degree in design and mechanical engineering from the National Institute of Applied Sciences (INSA) of Lyon in 2003. He received his PhD in acoustic in 2006 from University of Lyon. He is now an associate professor of mechatronics in the Mechanical Department of INSA-Lyon. His main research is done in the Contact and Structure Mechanics Laboratory. Main topics are about active/passive control of structures and energy harvesting.

Christophe Collette received his MSc and PhD degrees in mechanical engineering from the Université Libre de Bruxelles in 2003 and 2007. He is a professor of mechatronics in the Faculty of Engineering at the Université Libre de Bruxelles and University of Liège. He is the director of the Precision Mechatronics Laboratory. His main research interests include active and passive control of vibration, optical inertial sensors and future space telescopes.

Biographies of the other authors are not available.